A DISSERTATION FOR THE DEGREE OF MASTER OF SCIENCE

Integration of Ground Inventory Data with Landsat Imagery to Estimate Aboveground Biomass of Tropical Deciduous Forest in Bago Yoma, Myanmar

위성영상과 지상부 바이오매스 자료를 이용한

미안마 방고 요마 지역의 열대림 지상부 바이오매스 추정

BY

KHINE ZAW WYNN

DEPARTMENT OF FOREST SCIENCES

GRADUATE SCHOOL

SEOUL NATIONAL UINVERSITY

AUGUST 2015

A DISSERTATION FOR THE DEGREE OF MASTER OF SCIENCE

Integration of Ground Inventory Data with Landsat Imagery to Estimate Aboveground Biomass of Tropical Deciduous Forest in Bago Yoma, Myanmar

UNDER THE SUPERVISION OF ADVISER
PROF. HYUN SEOK KIM

SUMITTED TO THE FACULTY OF THE DEPARTMENT OF FOREST SCIENCES
SEOUL NATIONAL UNIVERSITY

PROGRAM IN FOREST ENVIRONMENTAL SCIENCE
DEPARTMENT OF FOREST SCIENCES
COLLEGE OF AGRICULTURE AND LIFE SCIENCES

AUGUST 2015

APPROVED AS A QUALIFIED DISSERTATION OF
KHINE ZAW WYNN

FOR THE DEGREE OF MASTER OF SCIENCE
BY THE COMMITTEE

CHAIRMAN _____

VICE CHAIRMAN _____

MEMBER _____

Abstract

Even with recently increased awareness of the environmental conservation, the degradation of tropical forests are still becoming the major source for carbon emission to the atmosphere. The aboveground biomass (AGB) of these forests are, therefore, a vital role in global carbon sequestration. As the initial step of the forest conservation in Myanmar, the aboveground biomass of South Zarmani Reserved Forest in Bago Yoma region were estimated using Landsat 8 OLI after the evaluation with 100 sample field inventory plots. Multiple linear regression (MLR) model of band values and their principal component analysis (PCA) model were developed to estimate the AGB using the spectral reflectance from Landsat images and elevation as the input variables. The MLR model had r^2 = 0.43, RMSE = 60.2 tons/ha, relative RMSE = 70.1%, Bias = -9.1 tons/ha, Bias (%) = -10.6%, and $p < 0.0001$, while the PCA model showed r^2 = 0.45, RMSE = 55.1 tons/ha, relative RMSE = 64.1%, Bias = -8.3 tons/ha, Bias (%) = -9.7%, and $p < 0.0001$. The AGB maps of the study area were generated based on both MLR and PCA models. The estimated mean AGB values were 74.74±22.3 tons/ha and 73.04±17.6 tons/ha and the total AGB of the study area are about 5.7 and 5.6 million tons from MLR and PCA, respectively. In conclusion, we were able to generate solid regression models from Landsat 8 OLI image after ground truth and two regression models gave us very similar AGB estimation (less than 2%) of South Zarmani Reserved Forest, Bago Yoma, Myanmar.

Keywords: aboveground biomass (AGB), Landsat 8 OLI, multiple linear regression (MLR), principal component analysis (PCA), tropical deciduous forest

Student ID: **2013-23876**

Table of Contents

Lists of Tables

Lists of Figures

Abbreviations

AGB	Aboveground Biomass
ALOS	Advanced Land Observing Satellite
AR-CDM	Afforestation and Reforestation - Clean Development Mechanism
ASTER	Advanced Spaceborne Thermal Emission and Reflection Radiometer
AVHRR	Advance Very High Resolution Radiometer
CO_2	Carbon dioxide
DN	Digital Numbers
DOS	Dark Object Subtraction
ETFRN	European Tropical Forest Research Network
ETM+	Enhanced Thematic Mapper Plus
FAO	Food and Agriculture Organization of the United Nations
FD	Forest Department
FRA	Forest Resources Assessment
GPS	Global Positioning System
HRSI	High Resolution Satellite Imagery
ITTO	International Tropical Timber Organization
LAI	Leaf Area Index
LiDAR	Light Detection and Ranging
Ln	Natural Logarithmic
MLR	Multiple Linear Regression

MODIS	Moderate Resolution Imaging Spectroradiometer
NIR	Near Infrared
NOAA	National Oceanic and Atmospheric Administration
OLI	Operational Land Imager
PALSAR	Phased Array L-band Synthetic Aperture Radar
PAN	Panchromatic
PCA	Principal Component Analysis
PIFs	Pseudo-invariant Features
Radar	Radio Detection and Ranging
REDD+	Reducing Emission from Deforestation and Forest Degradation
RS	Remote Sensing
SAR	Synthetic Aperture Radar
SCS	Sun-Canopy-Sensor
SWIR	Short Wave Infrared
TIRS	Thermal Infrared Sensor
TM	Thematic Mapper
UN	United Nations
USGS	United State Geological Survey
UTM	Universal Transverse Mercator
WGS	World Geodetic System
WRS	Worldwide Reference System

1. Introduction

Land cover change, which has accounted for ~20% of total CO_2 emission into atmosphere since the industrial revolution (Van Bodegom, Savenije, Wit, Boot, & Saile, 2009), decreased dramatically in temperate forest with recently increased awareness on environmental conservation and protection (Chakravarty, Ghosh, Suresh, Dey, & Shukla, 2012; FAO, 2010). However, deforestation in tropical forests are still occurring in many developing countries including Myanmar, mainly due to the economic reasons resulting about 13 million ha of tropical forests loss every year (FAO, 2010) and 6% - 17 % contribution of the global anthropogenic CO_2 emissions to the atmosphere (Baccini et al., 2012). As a consequence, tropical deforestations are significant net sources of CO_2 (e.g., J. T. Houghton, Meira Filho, Callander, Harris, and Kattenberg (1996); Watson et al. (2000)), even though tropical forests are considered as potential sinks of CO_2 due to their high capacity in photosynthesis (Malhi & Grace, 2000). In addition, tropical forests are home to more than half of the world's species and essential for global biogeochemical cycles (Nageswara-Rao, Soneji, & Sudarshana, 2012; Thomas & Baltzer, 2002). Therefore, tropical forests are important for both conservation and production.

For the protection of tropical forests, the accurate and efficient estimate of forest biomass, especially above ground biomass (AGB), is necessary. Conventional method using allometric equations and field collected data such as diameter at breast height (DBH) and tree height is considered as the most accurate method for AGB estimation, but it is time and labor consuming (Lu, 2006; Vicharnakorn, Shrestha, Nagai, Salam, & Kiratiprayoon, 2014; Zhu &

Liu, 2015). Therefore, remote sensing (RS) techniques after solid evaluation with ground truth are becoming the common and practical for AGB estimation, especially in large and remote areas (Avitabile, Baccini, Friedl, & Schmullius, 2012; Lu, 2006; Main-Knorn et al., 2011; Maynard, Lawrence, Nielsen, & Decker, 2007). For the estimation of AGB using RS data, a variety of direct and indirect approaches have been developed including multiple regression analysis (Steininger, 2000; D. Zheng et al., 2004), K nearest neighbor (Tomppo, Nilsson, Rosengren, Aalto, & Kennedy, 2002) , neural network (Foody, Boyd, & Cutler, 2003), principal component analysis (Ji et al., 2012), stochastic gradient boosting (Dube & Mutanga, 2015), Phua and Saito (2003) and Popescu, Wynne, and Nelson (2003) used canopy diameter and tree height which are derived from RS data to estimate biomass using multiple regression analysis. Although no methods can perform completely to estimate AGB (Vicharnakorn et al., 2014; Zhu & Liu, 2015), direct methods rather than indirect methods are widely used to estimate AGB in practice.

However, majority of studies have focused on AGB estimation in tropical forest in North and South America such as Amazon (e.g., Drake et al. (2003); R. A Houghton, Lawrence, Hackler, and Brown (2001); Lu (2005); Steininger (2000)) and relatively small number of studies were conducted in Africa and Asia (e.g., Baccini, Laporte, Goetz, Sun, and Dong (2008); Carreiras, Vasconcelos, and Lucas (2012); Dube and Mutanga (2015); He, Chen, An, and Li (2013); Manna et al. (2014)). Further, most of the studies in Asia were conducted in Bornean forest (e.g., Indonesia and Malaysia), which belongs to tropical rain forests (Foody et al., 2001; Kronseder, Ballhorn, Böhm, & Siegert,

2012; Morel et al., 2011). Only a few studies have conducted in tropical deciduous forests (e.g., Foody et al. (2003); Vicharnakorn et al. (2014)). About 37% of the Myanmar forest area, which covers about 47% of the country, is composed of tropical mixed deciduous forests (FD, 2010) and they are economically important since they include many valuable timber species, such as *Tectona grandis* (teak), *Xylia xylocarpa* (Pyinkado in Myanmar), *Terocarpus macrocarpus* (Padauk in Myanmar).

Recent fast growth of Myanmar economy since the change from socialism to capitalism in 2010 caused the increase of illegal logging and land cover change of forest areas, especially in tropical deciduous forest. Although there are several studies focus on AGB estimation in Myanmar, most of the studies conducted using destructive methods and they have limitations expending their outputs for the AGB estimation of large areas. Therefore, the objectives of our study are; (1) to develop the models to estimate the AGB of tropical deciduous forest in the Bago Yoma Region using RS techniques with ground truth evaluation, (2) to compare the performance of the multi linear regression analysis of bands value and principle component analysis models to estimate AGB in the study area, and (3) to generate the AGB distribution maps of the study area.

2. Literature Review

2.1. The role of tropical forests in climate change

Tropical forests are located in the 'tropics' which lie between the Tropic of Cancer and Capricorn, approximately between 23° N and 23° S latitudes (Thomas & Baltzer, 2002). Tropical Deciduous forests, about one-tenth of the world's land area (Nageswara-Rao et al., 2012) are rich in diversity and are important for both conservation and production. It is also important in terms of global biogeochemical cycles and are home to more than half of the world's species (Thomas & Baltzer, 2002).

Climate change is one of the major challenges of environmental concern in this century. Forests stored a lot of carbon from the atmosphere and the loss of forest tend to almost 20 percent of total emissions of carbon dioxide (Van Bodegom et al., 2009). Therefore, climate change and forests are closely related. The forestry sector plays a vital role in the global climate change mechanism. They have the potential to provide the several multi-benefits including biodiversity conservation, carbon sequestration and sustainable rural development (Fearnside, 1997).

Due to tropical forests play crucial role in determining the current atmospheric concentration of CO_2, as both sources of CO_2 following deforestation and sinks of CO_2 probably resulting from CO_2 stimulation of forest photosynthesis (Malhi & Grace, 2000), these forests are ecologically and environmentally important.

In recent years, the tropical forests are decreasing rapidly rate to deforestation and convert to other lands. These forests are being felled for

timber production and cleared for farming. Figure (1) showed estimated deforestation of tropical forests and temperate forests (FAO, 2012).

Nowadays, tropical forests ecosystems also face many potential threats due to climate change, including changed precipitation regimes and the increased incidence and severity of pests, diseases, fires and storms (ITTO, 2008). Climate change is becoming one of the greatest challenges in recent years. The impacts of climate change on tropical forests could affect the loss of natural resources, such as reducing the availability of forest products, traditional medicines for human well-being, and other services. Besides, the loss of tropical forests are alarming due to timber production, conversion to agriculture land, construction of roads and dams, pasture, firewood.

The forests (green plants) take carbon dioxide from the atmosphere and stored as carbon during photosynthesis. Hence, the forests are making a major contribution to mitigate the climate change. When the forests are burned or cut down, stored carbon is released into the atmosphere as carbon dioxide. Every year, more than 15 million hectares of tropical forests are cut down and millions of carbon tons is releasing into the atmosphere (www.nature.org). As a consequence, tropical forests are the major source of carbon emission to the atmosphere. Tropical forests, therefore, must be protected from deforestation and forest degradation if carbon emissions want to reduce from global warming. Many of the world's tropical forests will be lost alarming rate without protection now. The natural resources and important tropical species will be lost if the tropical forests lost.

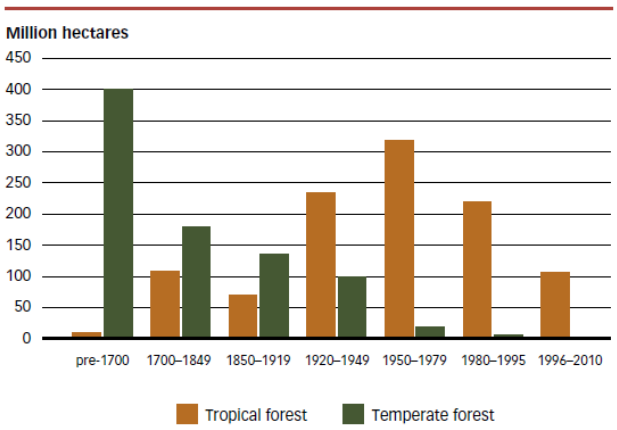

Figure 1. Estimated deforestation by the forest type and time period

2.2. Remote sensing approaches to estimation of AGB

Recently, remote sensing techniques are becoming useful tool in estimating forest structure and AGB production of forest and plantations. It also provides distribution of forest biomass from local, continental to global areas (Baccini, Friedl, Woodcock, & Warbington, 2004; R. A. Houghton et al., 2007; Lu, 2006; Zhang & Ni-meister, 2014; D. Zheng et al., 2004). Most of the studies in different parts of the world have examined the relationship between remote sensing and AGB. Landsat, LiDAR (light detection and ranging), MODIS (moderate resolution imaging spectroradiometer), and SAR (synthetic aperture radar) were used in estimating AGB as remotely sensed data.

Accurate estimates of biomass play a vital role in understanding the carbon cycle. Direct measurement of AGB require destructive sampling of trees(Brown, 1997). However, this method is not available to carry out for a large area. Hence, allometric equations which are developed from destructive method were used to estimate the AGB. Field surveys provide the most accurate method for obtaining vegetative data, but it is too time consuming and costly to

cover large expenses (Xie, Sha, Yu, Bai, & Zhang, 2009). Therefore, remotely sensed data acquired from satellite or aerial platforms has provided a practical and economical means to measure and monitor vegetation cover and structure, especially over a large areas (Xie, Sha, & Yu, 2008).

Three types of remote sensing data are often used to estimate AGB; passive optical remote sensing, radar (radio detection and ranging, microwave) data, and LiDAR (light detection and ranging) data. Optical spectral reflectance are sensitive to vegetation structure (leaf area index, crown size and tree density), texture and shadow, which are strongly correlated with AGB (Zhang & Ni-meister, 2014). Radar data are related to AGB through measuring dielectric and geometrical properties of forests (Le Toan et al., 2011). LiDAR remote sensing is promising in characterizing vegetation vertical structure and height which are then associated to AGB (Drake et al., 2002; Lefsky, Hudak, Cohen, & Acker, 2005).

The optical remote sensing data are commonly used for land cover mapping, biomass estimation, tree density. The forest biomass is estimated using spectral reflectance and vegetation indices from various satellite instruments of optical remote sensing. The empirical regression approaches (Hall, Skakun, Arsenault, & Case, 2006; Powell et al., 2010; D. Zheng et al., 2004) and nonlinear nonparametric approaches (Baccini et al., 2004; Fraser & Li, 2002) are developed to estimate forest biomass. The most frequently used optical remote sensing data may be the time series Landsat data, which have become the primary source in many applications, including AGB estimation at local and regional scales (Foody et al., 2003; Lu, 2005; Roy & Ravan, 1996;

Steininger, 2000; D. Zheng et al., 2004).

NOAA AVHRR (National Oceanic and Atmospheric Administration Advanced Very High Resolution Radiometer) and MODIS (Moderate Resolution Imaging Spectroradiometer) datasets at a spatial resolution from 250 m to 1.1 km are frequently used to produce biomass estimates at long term and global scales (Baccini et al., 2004; Baccini et al., 2008; Dong et al., 2003; Zhang & Kondragunta, 2006) while Landsat TM, Landsat ETM, Landsat 8 OLI, and Advanced Spaceborne Thermal Emission and Reflection Radiometer (ASTER) with a spatial resolution of 30 m are the most frequently used to estimate biomass at local and regional scales (Dube & Mutanga, 2015; Hall et al., 2006; Ji et al., 2012; Lu, 2005; Muukkonen & Heiskanen, 2005; G. Zheng, Chen, Tian, Ju, & Xia, 2007). The high resolution satellite imager (HSRI) on QuickBird with a spatial resolution of 2.44 m in multispectral and 0.61 m in panchromatic at nadir and IKONOS with a spatial resolution of 3.2 m in multispectral and 0.82 m in panchromatic are usually used to calculate the local tree biomass (Gonzalez et al., 2010; Leboeuf et al., 2007; Palace, Keller, Asner, Hagen, & Braswell, 2008).

Radar data physically measure biomass through the interaction of the radar waves with tree scattering elements (Zhang & Ni-meister, 2014). The widely used active radar data are from spaceborne synthetic aperture radar (SAR) sensors, such as the L-band ALOS PALSAR, the C-band ERS/SAR, RADARSAT/SAR or ENVISAT/SAR and the X-band TerraSAR-X instruments, which transmit microwave energy at wavelengths from 3.0 (X-band) to 23.6 cm (L-band). The proposed ESA Earth Explorer Mission

BIOMASS is the prime candidate to be the first P-band SAR satellite (Le Toan et al., 2011). The major advantage of all SAR systems is their weather- and daylight-independency. The ability of radar sensors to measure biomass mainly depend on how deep the radar signals can penetrate into the canopy. The longer the wavelength, the deeper the penetration (Englhart, Keuck, & Siegert, 2011; Le Toan et al., 2011).

Different radar data have their own characteristics in relating to forest stand parameters (Leckie & Ranson, 1998; Lu, 2006). For example, radar backscatter in the P and L bands is highly correlated with major forest parameters, such as tree age, tree height, DBH, basal area, and AGB. The SAR L-band data have proven to be valuable for AGB estimation (Kurvonen, Pulliainen, & Hallikainen, 1999; Luckman, Baker, Kuplich, Yanasse, & Frery, 1997; Sun, Ranson, & Kharuk, 2002). However, the SAR C-band and X-band were shown low correlations with AGB (Englhart et al., 2011; Le Toan, Beaudoin, Riom, & Guyon, 1992) while the higher correlation were found between SAR P-band backscatter and AGB (Le Toan et al., 2011).

Airborne LiDAR data are also used for estimating AGB (Baccini et al., 2012; Gonzalez et al., 2010; He et al., 2013; Kronseder et al., 2012). LiDAR is one of the most promising remote sensing technologies for estimating various biophysical properties of forests. LiDAR data are well suited to biomass estimation, as point clouds generated from forest canopies can accurately depict the physical characteristics of the canopy surface (Zhao, Guo, & Kelly, 2012). AGB is strongly related to LiDAR measured tree height, crown diameter, crown shape (He et al., 2013). In comparative studies, LiDAR has produced more

accurate estimates of forest biomass than optical satellite sensors (Gonzalez et al., 2010) and synthetic aperture radar sensors (Asner et al., 2012; Sexton, Bax, Siqueira, Swenson, & Hensley, 2009).

The radar or LiDAR data have important roles in AGB estimation, especially in study areas with frequent cloud conditions. However, the data analyses involved in pre-processing, removal of noise, and image processing require more skills, knowledge, and specific software. Also, the use of LiDAR data for large area monitoring is challenging because of operational considerations that limit widespread use, such as high data acquisition costs, aircraft scheduling and logistics, and large data volumes although accurate (Wulder, Bater, Coops, Hilker, & White, 2008).

The remote sensing data are commonly correlated to forest biomass using empirical regression models, non-parametric methods, and physically-based allometric models. Although LiDAR produced high accuracy in estimating AGB than Landsat data, LiDAR data have a limitation, such as high costs, availability. However, Landsat data can available get free and better to get cloud free or cloud least images. Hence, most of the research in different parts of the world were used Landsat data in estimating AGB.

3. Materials and Methods

3.1. Description of the Study Area

This study was carried out in South Zarmani Reserved Forest which belong to the tropical deciduous forest in Bago Yoma Region of Myanmar (Fig. 2). Geographic coordinates of this study area are 16° 50' 51" N and 96° 45' 28" E and the average elevation is about 300 m above sea level. There are two dam reservoirs, namely Zaungtu dam reservoir and Shwe Laung Kodu Kwe dam reservoir, inside the study area. This area is one of major timber producing area in Myanmar including valuable commercial timber species such as teak (*Tectona grandis*), pyinkado (*Xylia xylocarpa*), padauk (*Terocarpus macrocarpus*), *etc*. And also, local communities rely on forest products as the primary sources, such as timber, fuelwood, fodder. The study site covers an area of approximately 77000 ha. According to the nearest meteorological station, the mean annual temperature and rainfall of this area are 27.8 °C and 1323.2 mm. Alluvial soil is common in this study area (FD, 2012).

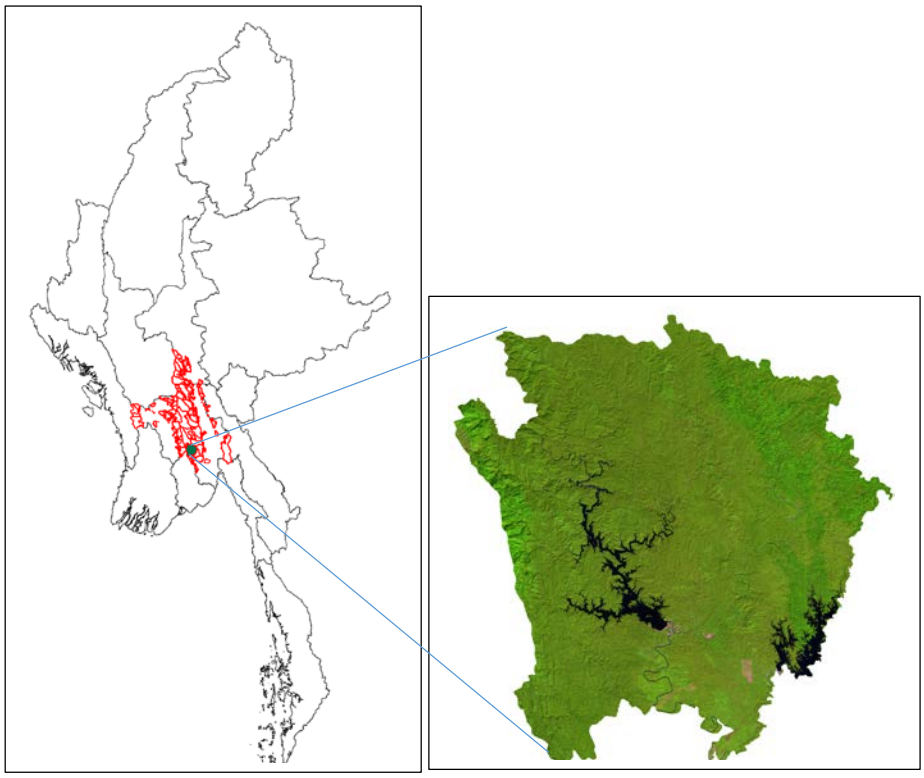

Figure 2. Location of the South Zarmani Reserved Forest

3.2. Remote Sensing Datasets

In this study, for the estimation of AGB, Landsat 8 OLI (2014) imagery was used. Because satellite goes over the same place on every 16 day, and it is better to get cloud free or cloud least image, Landsat image on clear day and about the same day of year in dry season were selected from 2014. Landsat 8 OLI image with less than 10% cloud cover were acquired on 24 Dec 2014. Conveniently, the study area was covered by one Landsat image (WRS-2, Path 132 and Row 48). Landsat 8 carries two instruments: the Operational Land Imager (OLI) sensor including nine spectral bands with a spatial resolution of 30 meters for Bands 1 to 7 and Band 9, while the spatial resolution

of Band 8 (panchromatic) is 15 meter and Thermal Infrared Sensor (TIRS) consisting of thermal bands 10 and 11 with a spatial resolution of 100 meters. The spectral bands and spatial resolution of Landsat 8 OLI image was expressed in Table 1.

At first, the Landsat images were georeferenced to the coordinate system of the study area (WGS 84, UTM projection, Zone 47 Q).The Landsat image was obtained in digital number (DN) and these DN value was transformed to reflectance value. The DN values of the Landsat 8 OLI were converted to the radiance data using the following equation given by https://landsat.usgs.gov/ Landsat8_Using_Product.php.

$$\mathbf{L_{sat} = M_L * Q_{cal} + A_L}$$

Where, L_{sat} is the at-satellite radiance, M_L is the band-specific multiplicative rescaling factor from Landsat metadata (RADIANCE_MULT_BAND_ x, where x is the band number), A_L is the band-specific additive rescaling factor from Landsat metadata (RADIANCE_ADD_BAND_x, where x is the band number), and Q_{cal} is the quantized and calibrated standard product pixel values (DN).

The USGS was also described that Landsat 8 images are provided with band-specific rescaling factors that allow for the direct conversion from DN to top of atmosphere (TOA) reflectance. However, the effects of the atmosphere should be considered in order to measure the reflectance at the ground. Therefore, the surface reflectance, ρ, was calculated using the dark object subtraction (DOS) equation described by Song, Woodcock, Seto, Lenney, and Macomber (2000);

$$\rho = (\pi (L_{sat} - L_p)) / T_v (E_0 \cos(\theta_z) T_z + E_{down})$$

where, L_p is the path radiance, T_v is the atmospheric transmittance from the target toward the sensor, E_0 is the exoatmospheric solar constant, E_{down} is the downwelling diffuse irradiance, θ_z is the solar zenith angle, and T_z is the atmospheric transmittance in the illumination direction. The assumption value of T_z, T_v and E_{down} in DOS are 1, 1, and 0, respectively according to (Song et al., 2000).

The path radiance L_p is calculated using the following equation;

$$L_p = G*DN_{min} + B - 0.01[E_0 \cos(\theta_z) T_z + E_{down}] T_v/\pi$$

Where, G is the sensor gain and B is the bias used for converting the sensor signals (DN) to at-satellite radiance. DN_{min} is the minimum darkest DN value.

The exoatmospheric solar constant, E0, is estimated using the following equation;

$$E_0 = (\pi d^2)* RADIANCE\_MAX / REFLECTANCE\_MAX$$

Where, d is the sun-earth distance, RADIANCE_MAX and REFLECTANCE_MAX are band-specific rescaling factors provided by image metadata.

Topographic correction is also necessary process in remote sensing technique for a mountainous areas (Gao et al., 2014; Gu & Gillespie, 1997; Wei, Qingjiu, & Liming, 2008). Due to the Bago Yoma is a mountainous region, topographic effect should also be considered one of the important factor. Therefore, topographic correction was done as below using the Sun-Canopy-Sensor correction model (SCS) provided by Gu and Gillespie (1997).

$$L/L_0 = A/A_0 = \cos\theta / \cos\theta_s \cos\alpha$$

Where, L is the radiance reflected from the direct solar irradiance of sloping pixel, L_0 is the radiance reflected from the direct solar irradiance, A is the total sunlit area of sloping pixel, A_0 is the total sunlit areal of level pixel, θ is the solar radiance incidence angle, θ_s is the sun zenith angle, and α is the terrain slope angle.

The solar radiance incidence angle, θ, can be calculated from

$$\cos \theta = \cos \theta_s \cos \alpha + \sin \theta_s \sin \alpha \cos \varphi$$

where, φ is the relative azimuth between the sun and the slope.

Table 1. Landsat 8 OLI spectral and spatial resolution

Landsat 8 OLI		
Bands	**Wavelength (micrometers)**	**Resolution (meters)**
Coastal	0.43 – 0.45	30
Blue	0.45 – 0.51	30
Green	0.53 – 0.59	30
Red	0.64 – 0.67	30
NIR	0.85 – 0.88	30
SWIR 1	1.57 – 1.65	30
SWIR 2	2.11 – 2.29	30
Pan	0.50 – 0.68	15
Cirrus	1.36 – 1.38	30
TIRS 1	10.60 – 11.19	100
TIRS 2	11.50 – 12.51	100

3.3. Field Biomass Measurement

The sample plots covering wide range of biomass were selected based on the normalized difference vegetation index (NDVI). Stratified random sampling design was used to determine the location of 100 sample plots using the global positioning system (GPS) in this study area (Fig. 3a) (Table 2). Each plot has a size of 900 m^2 (30 m x 30 m) and in this plot, trees with DBH ≥ 10 cm were recorded their diameter at breast height (DBH) and height (H) of all trees. At the center of each plot, sub plot 100 m^2 (10 m x 10 m) were established for measuring DBH and H of all trees with DBH < 10 cm. The sample plot design used in this study area was expressed in Figure 3b and the sample plots located in this study area was shown in Figure 3a. For each tree, the species names, diameter at breast height and height at ground level were recorded. Tree diameters were measured using diameter tape and tree heights were measured using Haglof ECII electronic clino meter. Data collection for this study were carried out from January to February 2015 in the dry season.

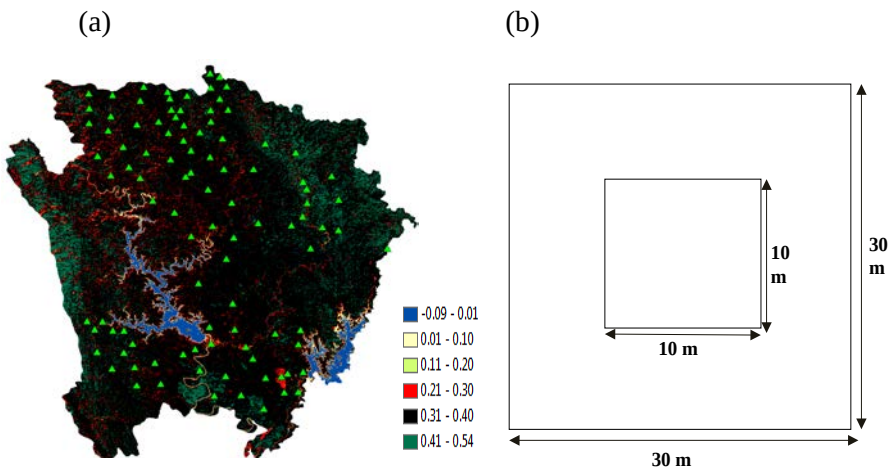

Figure 3. (a) Sample plots located in the study area and **(b)** Sample plot design used in this study

Table 2. Representative sample plots in each NDVI classes

No.	NDVI Classes	Stratified areas (ha)	No. of Sample Plots
1	Class 1	72.27	Water
2	Class 2	527.22	5
3	Class 3	719.01	5
4	Class 4	4556.34	15
5	Class 5	62777.34	55
6	Class 6	8876.88	20
	Total	**77529.06**	**100**

3.4. AGB Estimated from Field data

The total AGB for each plot were estimated using site specific equation for Bago Yoma Mountain which developed by Chan, Takeda, Suzuki, and Yamamoto (2013) using 68 tree species – covering most of our study trees - with the diameter greater than 1 cm. The allometric equation used for this study was as follow;

$$W = 0.064 \times (D^2H)^{0.862}$$

Where, W = biomass per tree in kg, D = diameter in breast height in cm and H = tree height in m. After generating tree level biomass, AGB of each sample plot was summed and converted into stand level total AGB (tons/plot and tons/ha).

3.5. Generating Regression Models for RS Biomass Estimation

To estimate the AGB of Bago Yoma region from RS, 56 out of 100 sample plots were used as the training plots for two different biomass estimation models. The first multiple linear regression model was developed using multiple satellite band values (Ripple, 1994; Xie et al., 2009; D. Zheng et al., 2004) and the second principle component regression model used its principle component values (Ji et al., 2012). Here after we call them MLR model and PCA model, respectively. The rest of 44 plots were used as test plots to check the validation of our models. The same training plots and testing plots were used for both MLR and PCA models. After the model development, AGB maps were generated from MLR and PCA models. For the model development, one dependent variable (AGB) and seven independent variables (B_2, B_3, B_4, B_5, B_6, B_7, and elevation data generated from the SRTM-90 m DEM downloaded from USGS) were used and went through stepwise regression analysis for selection of necessary variables. To reduce the error caused by the uncertainties in GPS, we used reflectance values, which were averaged within 3 x 3 window pixels centered on the GPS point of each field plot.

3.5.1. Multiple Linear Regression model (MLR)

MLR model for AGB estimation is based on the relationship between AGB and spectral bands.

$$\mathbf{Y = \alpha + \beta_1 B_2 + \beta_2 B_3 + \ldots\ldots + \beta_6 B_7 + \beta_7 Elevation}$$

Where, Y is the calculated AGB of training samples, α is the intercept, $\beta_{1\text{-}7}$ is

the slope coefficient of independent variables and B_{2-7} is the Landsat bands 2 to 7.

High collinearity between independent variables show statistical problem and therefore, collinearity between independent variables were examined by the variance inflation factor (VIF) and tolerance. High collinearity between independent variables occurs when tolerance < 0.20 or VIF > 4. To linear the relationship, AGB were converted to natural logarithmic form. The logarithmic regression is expressed as

$$\mathbf{Ln\ (Y) = \alpha + \beta_1 B_2 + \beta_2 B_3 + ... + \beta_6 B_7 + \beta_7 Elevation}$$

3.5.2. Principal Component Analysis (PCA)

Principal component analysis is a statistical procedure that the original correlated predictor variables were converted to new set of values of linearly uncorrelated variables, called the principal components (Jolliffe, 2002). The AGB estimation model is based on the AGB and spectral bands.

$$\mathbf{Y = \mathit{f}\ (B_2, B_3, B_4, B_5, B_6, B_7, Elevation) + e}$$

Where, Y is AGB, B_{1-9} is the spectral bands from Landsat image and e is error term. If the multicollinearity between independent variable occurs, it means that the high correlation among them. Therefore, to avoid multicollinearity between independent variables, PCA method were used. Thus, the regression is described as

$$\mathbf{Y = \mathit{f}\ (PC_1, PC_2, PC_3, PC_4, PC_5, PC_6, PC_7) + e}$$

Where, PC_{1-7} are principal component transformed from the seven independent variables. After that, to linearize the relationship between dependent variable

and independent variables, dependent variable (AGB) were converted to natural logarithmic form. Therefore, the regression is reconstructed to

$$\mathbf{Ln(Y) = b_0 + b_1PC_1 + b_2PC_2 + \ldots\ldots\ldots + b_7PC_7 + e}$$

Where, Ln(Y) is natural logarithmic of AGB, $b_{0\text{-}7}$ are the regression coefficient of independent variables.

The same training plots and testing plots were used for both MLR and PCA analysis. Training plots were used to generate MLR and PCA regression models and testing plots were used for model validation.

3.6. Model Validation

For the reliability of models performance, for both MLR and PCA models, the coefficient of determination (r^2), root mean square error (RMSE), relative RMSE, bias and bias (%) between observed values and predicted values were calculated using the following equations;

$$\boldsymbol{RMSE} = \sqrt{\frac{1}{n}\sum_{i=1}^{n}(X_{obs} - X_{model})^2}$$

$$\textbf{Relative RMSE} = (\textbf{RMSE} / \overline{X_{obs}}\ ) * 100$$

$$\boldsymbol{Bias} = \overline{X_{obs}} - \overline{X_{model}}$$

$$\textbf{Bias (\%)} = (\textbf{Bias} / \overline{X_{obs}}\ ) * 100$$

Where, X_{obs} is the observed AGB value using allometric equation, X_{model} is the modeled estimation from RS, $\overline{X_{obs}}$ is the mean of the observed value, and $\overline{X_{model}}$ is the mean of the predicted value.

4. Results and Discussion

4.1. Forest characteristics

There are total 3376 trees greater than 10 cm in diameter which belong to 110 species and 43 families from 100 (30m x 30m) sample plots. The ten most common species composition in 30m x 30m plots was shown Figure 4 and the all of the tree species are list in Appendix 1. *Tectona grandis* was the dominant species and it was followed *by Derris robusta* and *Lagerstroemia speciosa*. 73 species and the total of 679 trees were found from 100 (10m x 10m) sample plots. The ten most common species composition in 10m x 10m plots was shown in Figure 5 and the all of them are list in Appendix 2. *Mitragyna diversifolia* was the most dominant species and it was followed by *Lagerstroemia speciosa* and *Tectona grandis.*

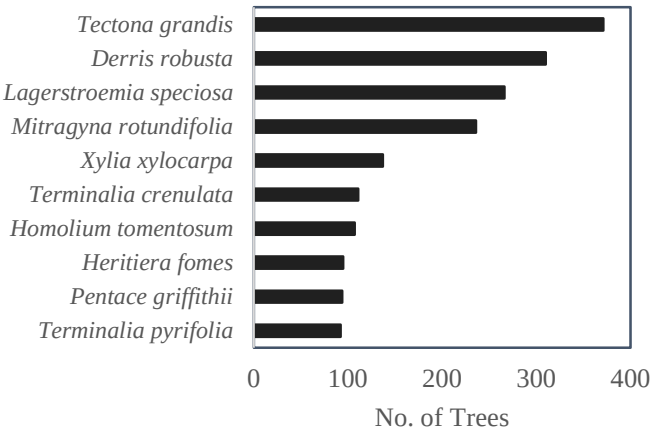

Figure 4. Ten most common species composition within 30m x 30m plots of the South Zarmani Reserved Forest

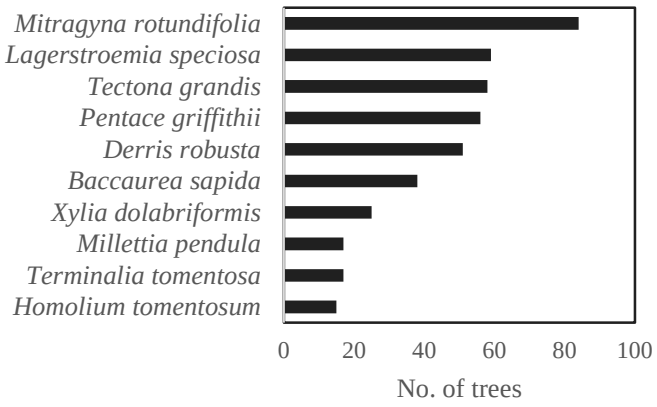

Figure 5. Ten most common species composition within 10m x 10m plots of the South Zarmani Reserved Forest

The basal area and stand density of the study area were 26.42±1.02 m^2/ha and 1054±72.86 trees/ha, respectively. Figure (6) and (7) show the distribution of basal area and distribution of tree numbers in the study area. These numbers are similar to other tropical Asia. Aye, Pampasit, Umponstira, Thanacharoenchanaphas, and Sasaki (2014) reported that the basal area and stand density of Popa Mountain Park in Myanmar were 27.5 m^2/ha and 1061 trees/ha, respectively. Kronseder et al. (2012) mentioned the basal area and stand density were 25.3±11.0 m^2/ha and 1074±819 trees/ha of lowland dipterocarp forest in Central Kalimantan, Borneo. Compared to tropical area in temperate forests, Gasparri, Parmuchi, Bono, Karszenbaum, and Montenegro (2010) showed the basal area ranged between 2.7 and 12.2 m2/h and stand density ranged from 74 to 265 trees/ha in Argentina. Gonzalez et al. (2010) resulted the stand density of 329±153 trees/ha, 333±157 trees/ha and 326±172 trees/ha in Garcia, Mailliard, and North Yuba, USA, respectively.

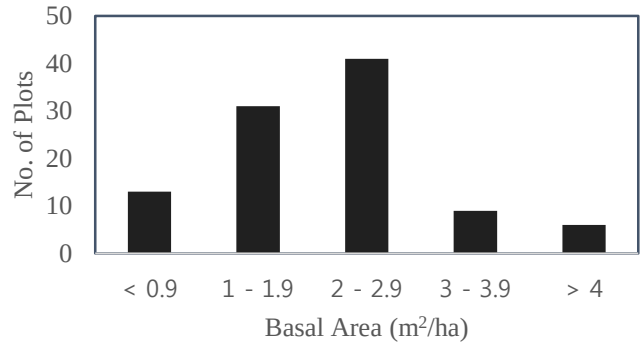

Figure 6. Distribution of basal area in the South Zarmani Reserved Forest

Figure 7. Distribution of tree numbers in the South Zarmani Reserved Forest

The numbers of trees and diameter distribution of all the trees in the 30m x 30m plots is given in Figure 8. It can be seen that the number of trees is decreasing when DBH gets larger. Therefore, it shows typical inverse J shape in the DBH distribution. Inside the 10m x 10m plots, the largest numbers of trees were occurred in 6-7.9 cm DBH class (Fig. 9). Figure 10 showed the height distribution of trees in the 30m x 30m plots. The number of trees categorizing in 5 to 9.9 m height class were greater than other height classes. Figure 11 represented the number of tress and height distribution of all trees in the 10m x 10m plots.

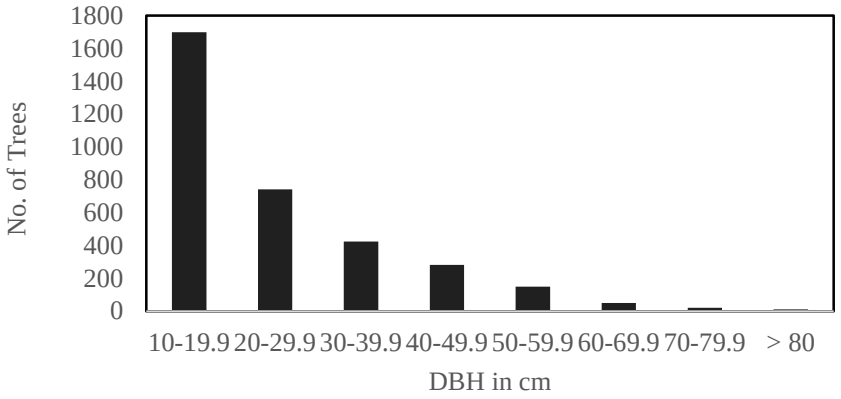

Figure 8. Diameter distribution within 30m x 30m plots of the South Zarmani Reserved Forest

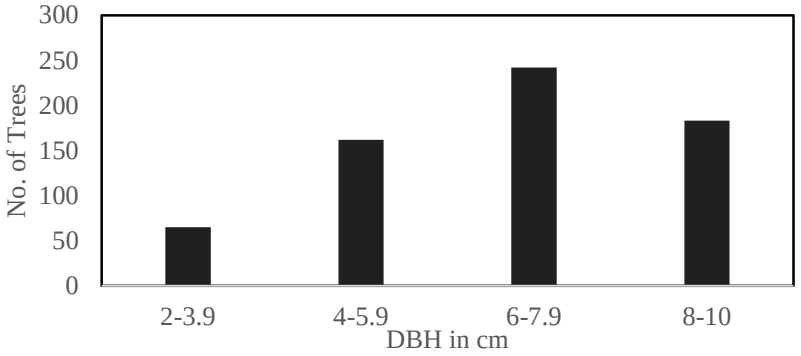

Figure 9. Diameter distribution within 10m x 10m plots of the South Zarmani Reserved Forest

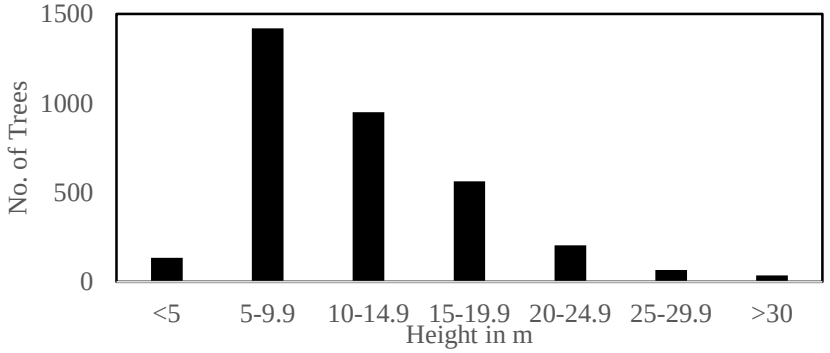

Figure 10. Height distribution within 30m x 30m plots of the South Zarmani Reserved Forest

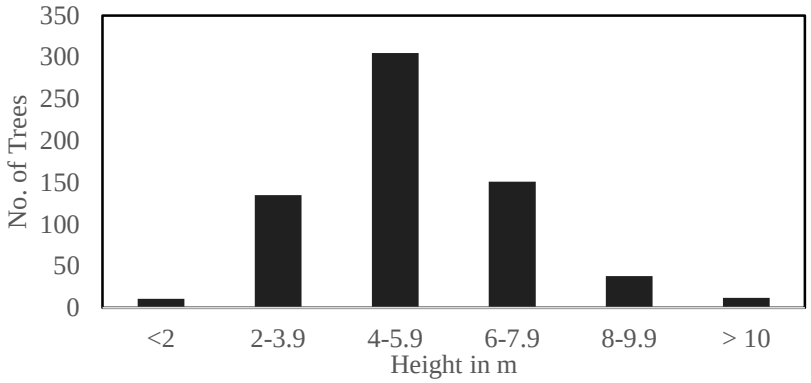

Figure 11. Height distribution within 10m x 10m plots of the South Zarmani Reserved Forest

4.2. AGB from Field Data

The AGB from field inventory data were estimated using site specific allometric equation from Chan et al. (2013). The results showed that high AGB and low AGB from field data were 330.54 tons/ha and 15.02 tons/ha, respectively. The descriptive statistics of training and test plots was expressed in Table 3. Compared with the previous studies, our study had a higher AGB value than other studies that were conducted in temperate and sub-tropical regions. Dube and Mutanga (2015) reported that the maximum value of AGB from field inventory data was 298.04 tons/ha in Africa. He et al. (2013) resulted the high value of AGB 174.88 tons/ha in China. Roy and Ravan (1996) mentioned 129.95 tons/ha as the high value of AGB from field data in India. However, our study had a lower AGB value when compared with the AGB value varies from 110 tons/ha to 500 tons/ha in Amazon (Lu, 2005).

Table 3. Descriptive Statistics of Training and Test Plots

Sample Plots	Min	Max	Mean	SD
Training Plots (56 plots)	15.02	252.99	82.26	26.74
Test Plots (44 plots)	21.66	330.54	85.95	34.29

4.3. Regression Models for AGB Estimation

When stepwise multiple regression was run to estimate the regression model using SPSS, high collinearity occurs between reflectance values of the spectral bands of the Landsat images (bands 2, 4, 6, and elevation). Therefore, these spectral bands were excluded from the independent variables. After that, the regression model were generated to estimate AGB from MLR. The regression model from MLR is expressed in Table 4.

Table 4. Regression models used for AGB estimation

Regression Model	R^2	*P*-Value	RMSE (tons/ ha)	RMSE (%)	Bias (tons/ ha)	Bias (%)
$\ln(AGB) = 31.103 - 161.882B_3 + 7.589B_5 + 43.866B_7$	0.43	0.0001	60.2	70.1	-9.1	-10.6
$\ln(AGB) = 4.254 - 0.043PC_1 - 0.89PC_4 + 16.698PC_5$	0.45	0.0001	55.1	64.1	-8.3	-9.7

In the PCA analysis, the results showed the eigenvalues of the first three PCs were 98.62% (70.90%, 15.91%, and 11.81% for PC_1, PC_2, PC_3, respectively) of the total variance, while the remaining four PCs were a little of

variance. Table 5 showed the correlation between variables and PCs (component matrix).

According to Table 5, PC_1 showed the highest loadings among all variables. The regression model for estimating AGB were calculated from PCA. This regression is described in Table 4.

Table 5. Component matrix of the principle components and variables

	PC1	PC2	PC3	PC4	PC5	PC6	PC7
Blue	0.978	0.143	-0.058	0.124	-0.012	0.064	0.003
Green	0.992	-0.010	0.053	0.042	-0.100	-0.039	0.009
Red	0.980	0.147	-0.083	0.079	0.059	-0.034	-0.029
NIR	0.300	-0.745	0.594	0.042	0.024	0.002	0.001
SWIR_1	0.973	-0.018	0.111	-0.198	-0.019	0.022	-0.018
SWIR_2	0.985	0.135	-0.044	-0.059	0.065	-0.012	0.035
Elevation	-0.235	0.706	0.668	0.009	0.001	-0.002	0.000

The relationship between observed AGB from field inventory data and predicted AGB from remote sensing based on MLR model and PCA model were moderately reliable showing y = 0.4635*observed ln(AGB) + 2.2954 (r^2 = 0.43, $p < 0.0001$) and y = 0.3709*observed ln(AGB) + 2.6614 (r^2 = 0.44, $p <$ 0.0001), respectively (Fig. 12). Dube and Mutanga (2015) estimated AGB using Landsat 8 OLI in Africa and reported an r^2 of 0.42. Gasparri et al. (2010) revealed an r^2 of 0.37 using Landsat images to estimate AGB in Argentina.

Compared with these previous studies using Landsat images, our study have a higher accuracy in estimating AGB.

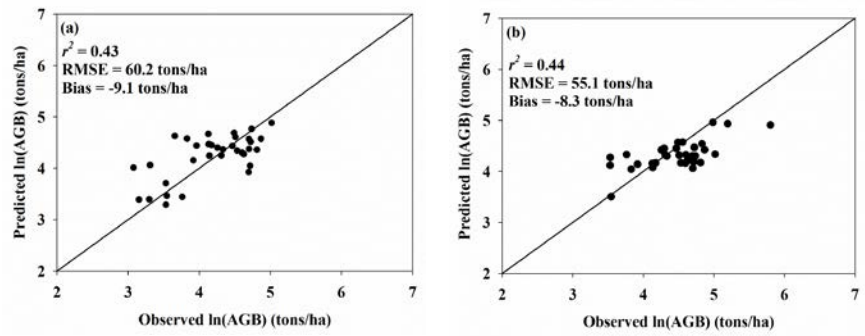

Figure 12. One to one relationship between observed ln(AGB) and predicted ln(AGB) based on: (a) MLR model and (b) PCA model

However, as shown in the regression relationship, the slope of the equations were significantly lower than one. Therefore, our models tended to underestimate the AGB at high biomass value at -10.6% in MLR model and -9.7% in PCA model (Table 4). However, the underestimation at high-end are common in other studies. For examples, Powell et al. (2010) developed three models to estimate AGB with underestimated value at -3% and -2.4% in gradient nearest neighbor (GNN) model and random forest (RF) model, respectively and overestimated value at 5.4% in reduced major axis (RMA) model in Minnesota, USA. Labrecque, Fournier, Luther, and Piercey (2006) reported that the BioCLUST model to estimate AGB was underestimated the value at -17 tons/ha when using the validation plots and -4 tons/ha when using the baseline map in Canada.

Our models RMSE (60.2 and 55.1 tons/ha in MLR and PCA, respectively) had a lower RMSE when compared with previous studies. Vicharnakorn et al. (2014) reported estimated AGB with RMSE 81.87 tons/ha in Lao PDR. Xie et al. (2009) described the RMSE 79.36 tons/ha for AGB estimation in Inner Mongolia. Luther, Fournier, Piercey, Guindon, and Hall (2006) revealed estimated AGB with a RMSE value of 63.6 tons/ha in the western Newfoundland ecoregion. Dube and Mutanga (2015) using Landsat 8 OLI images, showed estimated AGB with RMSE 66.41 tons/ha in South Africa.

Some other studies showed higher accuracy than our models; $r^2 = 0.67$ resulted by D. Zheng et al. (2004), $r^2 = 0.64$ described by Foody et al. (2001). The site specific allometric equation based on the DBH and height were only used in calculation of AGB estimation for this study. Therefore, the species specific allometric equation could be useful to improve the estimation of AGB. In order to improve the accuracy of AGB estimation, the leaf area index (LAI) and stand age should also be used in future estimation of AGB calculation. Other studies including leaf area index (LAI) and stand age as independent variable, showed the high accuracy in their model estimation. G. Zheng et al. (2007) described R^2 of 0.89 using LAI and stand age to estimate AGB in China. D. Zheng et al. (2004) revealed the AGB estimation model ($R^2 = 0.82$) using stand age and vegetation indices in USA. Therefore, we can assumed that the accuracy of AGB estimation can effectively improve using LAI and stand age. The data collection were carried out during a limited time and therefore, the LAI cannot measured in this study.

4.4. AGB Estimation Maps from Two Models

The regression model generated from MLR was first applied to produce AGB estimation map of the South Zarmani Reserved Forest. The results showed that estimated AGB is the range of values from 2.78 tons/ha to 236.69 tons/ha for the study area. There are totally about 5.7 million tons with the mean AGB of 74.74 tons/ha for the study area. Thematic AGB estimation map after classifying into four biomass categories was generated by using the regression results.

The AGB estimation map for the South Zarmani Reserved Forest was further generated using the regression model developed by PCA. The results showed that the value of estimated AGB varied from 0.000021 tons/ha to 214.67 tons/ha and the mean AGB is 73.04 tons/ha. There are totally about 5.6 million tons in the study area according to the estimation results and the four biomass categories were reclassified from the thematic AGB estimation map generated by using PCA model.

The highest biomass value 236 tons/ha from MLR model is a relatively high when compare the highest value 214 tons/ha from PCA model. Figure 13 shows the comparison of thematic AGB estimation map between MLR and PCA models. The areas of representative biomass categories analysis from MLR and PCA were shown in Table 6.

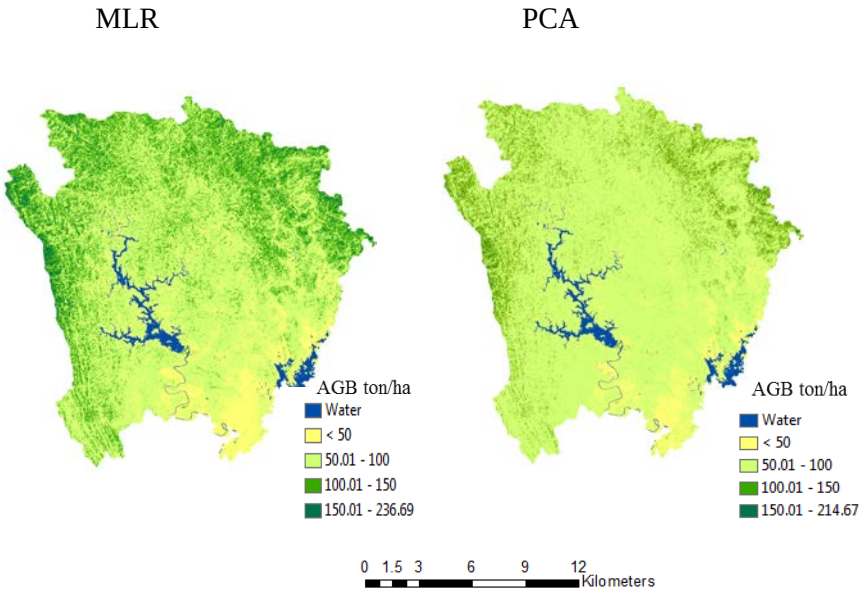

Figure 13. Comparison of AGB estimation map developed from MLR and PCA

Table 6. Representative areas of four biomass categories from MLR and PCA

Biomass Categories	**Area(ha)**
Less than 50 tons/ha	10907.64
50 - 100 tons/ha	46828.80
100 - 150 tons/ha	17215.02
> 150 tons/ha	2505.33
Total	**77456.79**

Biomass Categories	**Area(ha)**
Less than 50 tons/ha	6917.40
50 - 100 tons/ha	57600.18
100 - 150 tons/ha	12142.80
> 150 tons/ha	796.41
Total	**77456.79**

Similarly in both MLR and PCA, AGB estimation using field inventory data and Landsat 8 OLI, had the highest proportion in the category of 50 – 100 tons/ha and that of more than 150 tons/ha biomass category was relatively low (Table 6). The mean AGB from MLR is 74.74 tons/ha and the total AGB of the study area was about 5.7 million tons. The mean AGB from PCA is 73.04 tons/ha and the total AGB was about 5.6 million tons, which is similar with MLR. Although the highest biomass (tons/ha) was more than 330 tons/ha calculated from field inventory data, MLR generated 236 tons/ha and PCA generated 214 tons/ha as highest biomass values. Although the MLR model was generated the highest estimated AGB value than PCA model, PCA model had a lower RMSE, relative RMSE, bias and bias (%) than MLR. The results found that the value of estimated AGB using Landsat images was relatively lower than the biomass value calculated from field inventory data.

In compare with other AGB estimation of different study area, the results found that the mean value of estimated AGB 74.74 tons/ha derived from MLR and 73.04 tons/ha generated from PCA were similar to other studies. Dube and Mutanga (2015) showed that the mean value of estimated AGB 55.32 tons/ha using Landsat 8 OLI in South Africa. Roy and Ravan (1996) resulted estimated mean AGB 45.49 tons/ha in India. The estimated mean AGB values 82.71 Mg/ha in Bornean forest described by Englhart et al. (2011).

In this study, the calculation of estimated AGB depends only on the two dimensional approaches such as Landsat images, so there should be used three dimensional approaches such as aerial photo, radar and LiDAR images to improve the accuracy of the AGB estimation. He et al. (2013) described an R^2

of 0.74 using LiDAR data to estimate AGB in China. Kronseder et al. (2012) mentioned that the AGB were estimated an R^2 of 0.71 using LiDAR data in Borneo. Although these instruments have more powerful to accurate the estimation of AGB, these datasets have a limitation due to high costs, availability, huge data-volume as well as high data pre-processing costs (Dube & Mutanga, 2015). The Landsat images, therefore, are more suitable to estimate AGB for regional scale.

5. Conclusion

South Zarmani Reserved Forest is an important forest type which producing the valuable timber species in Myanmar. However, due to overexploitation and illegal logging, deforestation and forest degradation were increasing rapidly rate in this area. However, there is no systematic studies to estimate the AGB and to produce AGB map for this area till now. Therefore, AGB estimation and AGB map were generated for this area using field inventory data and Landsat data. Mapping the aboveground biomass for this area is an important to support the study of the deforestation and forest degradation and social-economic environment.

Moreover, this study has developed two models, MLR and PCA, for predicting aboveground biomass. Both models gave a good precision for estimating AGB and are applicable to map AGB for the study area. In comparing two models, PCA model generated lower RMSE, relative RMSE, bias and bias (%), higher r^2, and more accuracy in estimating AGB than the MLR model. The MLR and PCA models to estimate the AGB were based on the spectral bands derived from Landsat images and elevation. According to Figure 12, the results showed that the observed AGB from field inventory data is correlated fairly with the predicted AGB from Landsat images. The AGB maps derived from PCA and MLR model are useful for future forest management in Myanmar.

The highest value of estimated AGB was more than 330 tons/ha calculated from field inventory data, while 214 tons/ha were generated from PCA model and 236 tons/ha from MLR model as the highest estimated AGB

value, respectively. The results revealed that the estimated AGB value from PCA model were relatively lower than estimated AGB value from MLR model, whereas both models were estimated the AGB value lower than the field inventory data. However, other studies suggested that our models can be improve if other independent variables such as LiDAR based canopy height, stand age, and LAI are included, aerial photos datasets.

In conclusion, aboveground biomass is an important variable for national greenhouse inventory and carbon mitigation projects, particularly tree based projects. AGB can be used indicator for the degraded state of the forest ecosystem and also, correlated to the carbon content of the tree species. Therefore, AGB is useful for estimating the effectiveness of ecosystems as carbon sink. This study can provide to estimate the carbon emission due to deforestation and forest degradation. Moreover, this kind of study would also be applicable for the CDM and REDD+ mechanism in Myanmar, especially in Bago Yoma Region.

Literatures Cited

Asner, G. P., Mascaro, J., Muller-Landau, H. C., Vieilledent, G., Vaudry, R., Rasamoelina, M., . . . van Breugel, M. (2012). A universal airborne LiDAR approach for tropical forest carbon mapping. *Oecologia, 168*(4), 1147-1160.

Avitabile, V., Baccini, A., Friedl, M. A., & Schmullius, C. (2012). Capabilities and limitations of Landsat and land cover data for aboveground woody biomass estimation of Uganda. *Remote Sensing of Environment, 117*, 366-380.

Aye, Y. Y., Pampasit, S., Umponstira, C., Thanacharoenchanaphas, K., & Sasaki, N. (2014). Estimation of Carbon Emission Reductions by Managing Dry Mixed Deciduous Forest: Case Study in Popa Mountain Park. *Low Carbon Economy, 05*(02), 80-93. doi: 10.4236/lce.2014.52009

Baccini, A., Friedl, M., Woodcock, C., & Warbington, R. (2004). Forest biomass estimation over regional scales using multisource data. *Geophysical research letters, 31*(10).

Baccini, A., Goetz, S. J., Walker, W. S., Laporte, N. T., Sun, M., Sulla-Menashe, D., . . . Houghton, R. A. (2012). Estimated carbon dioxide emissions from tropical deforestation improved by carbon-density maps. *Nature Climate Change, 2*(3), 182-185. doi: 10.1038/nclimate1354

Baccini, A., Laporte, N., Goetz, S. J., Sun, M., & Dong, H. (2008). A first map of tropical Africa's above-ground biomass derived from satellite imagery. *Environmental Research Letters, 3*(4), 045011. doi: 10.1088/1748-9326/3/4/045011

Brown, S. (1997). *Estimating biomass and biomass change of tropical forests: A Primer* (Vol. 134): Food & Agriculture Organization. Rome.

Carreiras, J. M. B., Vasconcelos, M. J., & Lucas, R. M. (2012). Understanding the relationship between aboveground biomass and ALOS PALSAR data in the forests of Guinea-Bissau (West Africa). *Remote Sensing of Environment, 121*, 426-442. doi: 10.1016/j.rse.2012.02.012

Chakravarty, S., Ghosh, S., Suresh, C., Dey, A., & Shukla, G. (2012). *Deforestation: causes, effects and control strategies*: ISBN.

Chan, N., Takeda, S., Suzuki, R., & Yamamoto, S. (2013). Establishment of allometric models and estimation of biomass recovery of swidden cultivation fallows in mixed deciduous forests of the Bago Mountains, Myanmar. *Forest Ecology and Management, 304*, 427-436. doi: DOI 10.1016/j.foreco.2013.05.038

Dong, J., Kaufmann, R. K., Myneni, R. B., Tucker, C. J., Kauppi, P. E., Liski, J., . . . Hughes, M. K. (2003). Remote sensing estimates of boreal and temperate forest woody biomass: carbon pools, sources, and sinks. *Remote Sensing of Environment, 84*(3), 393-410.

Drake, J. B., Dubayah, R. O., Clark, D. B., Knox, R. G., Blair, J. B., Hofton, M. A., . . . Prince, S. (2002). Estimation of tropical forest structural characteristics using large-footprint lidar. *Remote Sensing of Environment, 79*(2), 305-319.

Drake, J. B., Knox, R. G., Dubayah, R. O., Clark, D. B., Condit, R., Blair, J. B., & Hofton, M. (2003). Above-ground biomass estimation in closed canopy neotropical forests using lidar remote sensing: factors affecting

the generality of relationships. *Global Ecology and Biogeography, 12*(2), 147-159.

Dube, T., & Mutanga, O. (2015). Evaluating the utility of the medium-spatial resolution Landsat 8 multispectral sensor in quantifying aboveground biomass in uMgeni catchment, South Africa. *ISPRS Journal of Photogrammetry and Remote Sensing, 101*, 36-46. doi: 10.1016/j.isprsjprs.2014.11.001

Englhart, S., Keuck, V., & Siegert, F. (2011). Aboveground biomass retrieval in tropical forests — The potential of combined X- and L-band SAR data use. *Remote Sensing of Environment, 115*(5), 1260-1271. doi: 10.1016/j.rse.2011.01.008

FAO. (2010). *Global Forest Resources Assessment 2010 FAO. Main Report*: FAO Forest Paper 163. Rome, Italy. 378 pp.

FAO. (2012). *State of the World's Forest 2012* FAO, Rome. 60 pp.

FD. (2010). *Forestry in Myanmar 2010*. Forest Department. 57 pp.

FD. (2012). *Bago District Forest Management Plan 2012-2013*: Forest Department, Myanmar. (Text in Myanmar).

Fearnside, P. M. (1997). Wood density for estimating forest biomass in Brazilian Amazonia. *Forest Ecology and Management, 90*(1), 59-87. doi: Doi 10.1016/S0378-1127(96)03840-6

Foody, G. M., Boyd, D. S., & Cutler, M. E. J. (2003). Predictive relations of tropical forest biomass from Landsat TM data and their transferability between regions. *Remote Sensing of Environment, 85*(4), 463-474. doi: Doi 10.1016/S0034-4257(03)00039-7

Foody, G. M., Cutler, M. E., Mcmorrow, J., Pelz, D., Tangki, H., Boyd, D. S., & Douglas, I. (2001). Mapping the biomass of Bornean Tropical rain forest from remotely senesd data. *Global Ecology and Biogeography, 10*, 379-387.

Fraser, R., & Li, Z. (2002). Estimating fire-related parameters in boreal forest using SPOT VEGETATION. *Remote Sensing of Environment, 82*(1), 95-110.

Gao, M.-L., Zhao, W.-J., Gong, Z.-N., Gong, H.-L., Chen, Z., & Tang, X.-M. (2014). Topographic Correction of ZY-3 Satellite Images and Its Effects on Estimation of Shrub Leaf Biomass in Mountainous Areas. *Remote Sensing, 6*(4), 2745-2764. doi: 10.3390/rs6042745

Gasparri, N. I., Parmuchi, M. G., Bono, J., Karszenbaum, H., & Montenegro, C. L. (2010). Assessing multi-temporal Landsat 7 ETM+ images for estimating above-ground biomass in subtropical dry forests of Argentina. *Journal of Arid Environments, 74*(10), 1262-1270.

Gonzalez, P., Asner, G. P., Battles, J. J., Lefsky, M. A., Waring, K. M., & Palace, M. (2010). Forest carbon densities and uncertainties from Lidar, QuickBird, and field measurements in California. *Remote Sensing of Environment, 114*(7), 1561-1575.

Gu, D., & Gillespie, A. (1997). Topographic normalization of Landsat TM images of forest based on subpixel Sun-Canopy-Sensor geometry. *Remote Sensing of Environment, 64*, 166-175.

Hall, R. J., Skakun, R. S., Arsenault, E. J., & Case, B. S. (2006). Modeling forest stand structure attributes using Landsat ETM+ data: Application

to mapping of aboveground biomass and stand volume. *Forest Ecology and Management, 225*(1-3), 378-390. doi: 10.1016/j.foreco.2006.01.014

He, Q., Chen, E., An, R., & Li, Y. (2013). Above-Ground Biomass and Biomass Components Estimation Using LiDAR Data in a Coniferous Forest. *Forests, 4*(4), 984-1002. doi: 10.3390/f4040984

Houghton, J. T., Meira Filho, L., Callander, B., Harris, N., & Kattenberg, A. (1996). *Climate change 1995: the science of climate change*: Cambridge University Press, Cambridge, New York. 572 pp.

Houghton, R. A., Butman, D., Bunn, A. G., Krankina, O. N., Schlesinger, P., & Stone, T. A. (2007). Mapping Russian forest biomass with data from satellites and forest inventories. *Environmental Research Letters, 2*(4), 045032.

Houghton, R. A., Lawrence, K. T., Hackler, J. L., & Brown, S. (2001). The spatial distribution of forest biomass in the Brazilian Amazon: a comparison of estimates. *Glob Chang Biol, 7*(7), 731-746. doi: DOI 10.1046/j.1365-2486.2001.00426.x

ITTO. (2008). *Tropical Forests and Climate Change: Internaional Expert Meeting on Addressing Climate Change through Sustainable Management of Tropical Forests*: Yokohama, Japan, 30 April - 2 May 2008. 62 pp.

Ji, L., Wylie, B. K., Nossov, D. R., Peterson, B., Waldrop, M. P., McFarland, J. W., . . . Hollingsworth, T. N. (2012). Estimating aboveground biomass in interior Alaska with Landsat data and field measurements.

International Journal of Applied Earth Observation and Geoinformation, 18, 451-461. doi: DOI 10.1016/j.jag.2012.03.019

Jolliffe, I. (2002). *Principal component analysis*: Wiley Online Library.

Kronseder, K., Ballhorn, U., Böhm, V., & Siegert, F. (2012). Above ground biomass estimation across forest types at different degradation levels in Central Kalimantan using LiDAR data. *International Journal of Applied Earth Observation and Geoinformation, 18*, 37-48. doi: 10.1016/j.jag.2012.01.010

Kurvonen, L., Pulliainen, J., & Hallikainen, M. (1999). Retrieval of biomass in boreal forests from multitemporal ERS-1 and JERS-1 SAR images. *Geoscience and Remote Sensing, IEEE Transactions on, 37*(1), 198-205.

Labrecque, S., Fournier, R. A., Luther, J. E., & Piercey, D. (2006). A comparison of four methods to map biomass from Landsat-TM and inventory data in western Newfoundland. *Forest Ecology and Management, 226*(1-3), 129-144. doi: 10.1016/j.foreco.2006.01.030

Le Toan, T., Beaudoin, A., Riom, J., & Guyon, D. (1992). Relating forest biomass to SAR data. *Geoscience and Remote Sensing, IEEE Transactions on, 30*(2), 403-411.

Le Toan, T., Quegan, S., Davidson, M., Balzter, H., Paillou, P., Papathanassiou, K., . . . Shugart, H. (2011). The BIOMASS mission: Mapping global forest biomass to better understand the terrestrial carbon cycle. *Remote Sensing of Environment, 115*(11), 2850-2860.

Leboeuf, A., Beaudoin, A., Fournier, R., Guindon, L., Luther, J., & Lambert,

M.-C. (2007). A shadow fraction method for mapping biomass of northern boreal black spruce forests using QuickBird imagery. *Remote Sensing of Environment, 110*(4), 488-500.

Leckie, D., & Ranson, K. (1998). Forestry applications using imaging radar. *Principles and Applications of Imaging Radar, 2*, 435-509.

Lefsky, M. A., Hudak, A. T., Cohen, W. B., & Acker, S. (2005). Geographic variability in lidar predictions of forest stand structure in the Pacific Northwest. *Remote Sensing of Environment, 95*(4), 532-548.

Lu, D. (2005). Aboveground biomass estimation using Landsat TM data in the Brazilian Amazon. *International Journal of Remote Sensing, 26*(12), 2509-2525. doi: 10.1080/01431160500142145

Lu, D. (2006). The potential and challenge of remote sensing-based biomass estimation. *International Journal of Remote Sensing, 27*(7), 1297-1328. doi: 10.1080/01431160500486732

Luckman, A., Baker, J., Kuplich, T. M., Yanasse, C. d. C. F., & Frery, A. C. (1997). A study of the relationship between radar backscatter and regenerating tropical forest biomass for spaceborne SAR instruments. *Remote Sensing of Environment, 60*(1), 1-13.

Luther, J., Fournier, R., Piercey, D., Guindon, L., & Hall, R. (2006). Biomass mapping using forest type and structure derived from Landsat TM imagery. *International Journal of Applied Earth Observation and Geoinformation, 8*(3), 173-187.

Main-Knorn, M., Moisen, G. G., Healey, S. P., Keeton, W. S., Freeman, E. A., & Hostert, P. (2011). Evaluating the Remote Sensing and Inventory-

Based Estimation of Biomass in the Western Carpathians. *Remote Sensing, 3*(12), 1427-1446. doi: 10.3390/rs3071427

Malhi, Y., & Grace, J. (2000). Tropical forests and atmospheric carbon dioxide. *Tree, 15*.

Manna, S., Nandy, S., Chanda, A., Akhand, A., Hazra, S., & Dadhwal, V. K. (2014). Estimating aboveground biomass in Avicennia marinaplantation in Indian Sundarbans using high-resolution satellite data. *Journal of Applied Remote Sensing, 8*(1), 083638. doi: 10.1117/1.jrs.8.083638

Maynard, C., Lawrence, R., Nielsen, G., & Decker, G. (2007). Modeling Vegetation Amount Using Bandwise Regression and Ecological Site Descriptions as an Alternative to Vegetation Indices. *GIScience & Remote Sensing, 44*(1), 68-81. doi: 10.2747/1548-1603.44.1.68

Morel, A. C., Saatchi, S. S., Malhi, Y., Berry, N. J., Banin, L., Burslem, D., . . . Ong, R. C. (2011). Estimating aboveground biomass in forest and oil palm plantation in Sabah, Malaysian Borneo using ALOS PALSAR data. *Forest Ecology and Management, 262*(9), 1786-1798.

Muukkonen, P., & Heiskanen, J. (2005). Estimating biomass for boreal forests using ASTER satellite data combined with standwise forest inventory data. *Remote Sensing of Environment, 99*(4), 434-447.

Nageswara-Rao, M., Soneji, J. R., & Sudarshana, P. (2012). *Structure, diversity, threats and conservation of Tropical Forests*: INTECH Open Access Publisher.

Palace, M., Keller, M., Asner, G. P., Hagen, S., & Braswell, B. (2008). Amazon

forest structure from IKONOS satellite data and the automated characterization of forest canopy properties. *BIOTROPICA, 40*(2), 141-150.

Phua, M.-H., & Saito, H. (2003). Estimation of biomass of a mountainous tropical forest using Landsat TM data. *Canadian Journal of Remote Sensing, 29*(4), 429-440.

Popescu, S. C., Wynne, R. H., & Nelson, R. F. (2003). Measuring individual tree crown diameter with lidar and assessing its influence on estimating forest volume and biomass. *Canadian Journal of Remote Sensing, 29*(5), 564-577.

Powell, S. L., Cohen, W. B., Healey, S. P., Kennedy, R. E., Moisen, G. G., Pierce, K. B., & Ohmann, J. L. (2010). Quantification of live aboveground forest biomass dynamics with Landsat time-series and field inventory data: A comparison of empirical modeling approaches. *Remote Sensing of Environment, 114*(5), 1053-1068.

Ripple, W. J. (1994). Determining coniferous forest cover and forest fragmentation with NOAA-9 Advanced Very High Resolution Radiometer data. *Photogrammetric Engineering and Remote Sensing, 60*(5).

Roy, P. S., & Ravan, S. A. (1996). Biomass estimation using satellite remote sensing data—An investigation on possible approaches for natural forest. *J. Biosci.,, 21*, 535-561.

Sexton, J. O., Bax, T., Siqueira, P., Swenson, J. J., & Hensley, S. (2009). A comparison of lidar, radar, and field measurements of canopy height in

pine and hardwood forests of southeastern North America. *Forest Ecology and Management, 257*(3), 1136-1147.

Song, C., Woodcock, C. E., Seto, K. C., Lenney, M. P., & Macomber, S. (2000). Classification and change detection using Landsat TM data: When and How to correct atmospheric effects? *Remote Sensing of Environment, 75*, 230-244.

Steininger, M. K. (2000). Satellite estimation of tropical secondary forest above-ground biomass: Data from Brazil and Bolivia. *International Journal of Remote Sensing, 21*(6-7), 1139-1157. doi: 10.1080/014311600210119

Sun, G., Ranson, K., & Kharuk, V. (2002). Radiometric slope correction for forest biomass estimation from SAR data in the Western Sayani Mountains, Siberia. *Remote Sensing of Environment, 79*(2), 279-287.

Thomas, S. C., & Baltzer, J. L. (2002). Tropical Forests. *Encyclopedia of Life Sciences*, 1-8.

Tomppo, E., Nilsson, M., Rosengren, M., Aalto, P., & Kennedy, P. (2002). Simultaneous use of Landsat-TM and IRS-1C WiFS data in estimating large area tree stem volume and aboveground biomass. *Remote Sensing of Environment, 82*(1), 156-171.

Van Bodegom, A. J., Savenije, H., Wit, M., Boot, R., & Saile, P. (2009). *Forests and climate change: adaptation and mitigation*: European Tropical Forest Research Network (ETFRN).

Vicharnakorn, P., Shrestha, R. P., Nagai, M., Salam, A. P., & Kiratiprayoon, S. (2014). Carbon Stock Assessment Using Remote Sensing and Forest

Inventory Data in Savannakhet, Lao PDR. *Remote Sensing, 6*(6), 5452-5479. doi: DOI 10.3390/rs6065452

Watson, R. T., Noble, I. R., Bolin, B., Ravindranath, N. H., Verardo, D. J., & Dokken, D. J. (2000). *Land use, land-use change and forestry: a special report of the Intergovernmental Panel on Climate Change*: Cambridge University Press, Cambridge, UK. 377 pp.

Wei, C., Qingjiu, T., & Liming, W. (2008). A model of topographic correction and reflectance retrieval for optical satellite data in forested areas. *The International Archives of the Photogrammetry, Remote Sensing and Spatial Information Sciences (ISPRC). Beijing China*, 243-248.

Wulder, M. A., Bater, C. W., Coops, N. C., Hilker, T., & White, J. C. (2008). The role of LiDAR in sustainable forest management. *The Forestry Chronicle, 84*.

Xie, Y., Sha, Z., & Yu, M. (2008). Remote sensing imagery in vegetation mapping: a review. *Journal of plant ecology, 1*(1), 9-23.

Xie, Y., Sha, Z., Yu, M., Bai, Y., & Zhang, L. (2009). A comparison of two models with Landsat data for estimating above ground grassland biomass in Inner Mongolia, China. *Ecological Modelling, 220*(15), 1810-1818. doi: 10.1016/j.ecolmodel.2009.04.025

Zhang, X., & Kondragunta, S. (2006). Estimating forest biomass in the USA using generalized allometric models and MODIS land products. *Geophysical research letters, 33*(9).

Zhang, X., & Ni-meister, W. (2014). Remote Sensing of Forest Biomass *Biophysical Applications of Satellite Remote Sensing* (pp. 63-98):

Springer.

Zhao, F., Guo, Q., & Kelly, M. (2012). Allometric equation choice impacts lidar-based forest biomass estimates: A case study from the Sierra National Forest, CA. *Agricultural and Forest Meteorology, 165*, 64-72.

Zheng, D., Rademacher, J., Chen, J., Crow, T., Bresee, M., Le Moine, J., & Ryu, S.-R. (2004). Estimating aboveground biomass using Landsat 7 ETM+ data across a managed landscape in northern Wisconsin, USA. *Remote Sensing of Environment, 93*(3), 402-411. doi: 10.1016/j.rse.2004.08.008

Zheng, G., Chen, J. M., Tian, Q. J., Ju, W. M., & Xia, X. Q. (2007). Combining remote sensing imagery and forest age inventory for biomass mapping. *J Environ Manage, 85*(3), 616-623. doi: 10.1016/j.jenvman.2006.07.015

Zhu, X., & Liu, D. (2015). Improving forest aboveground biomass estimation using seasonal Landsat NDVI time-series. *ISPRS Journal of Photogrammetry and Remote Sensing, 102*, 222-231. doi: 10.1016/j.isprsjprs.2014.08.014

Appendix 1

List of species found inside 30m x 30m plots of South Zarmani Reserved Forest

Myanmar Names	Botanical Names	Family Names
Aukchinsa	*Amoora wallichii* King	Meliaceae
Baing	*Tetramales nudiflora* R, Br.	Tetramelaceae
Bamaw	*Elaeocarpus wallichii* Kurz	Elaeocarpaceae
Bantbway	*Careya arborea* Roxb.	Lecythidaceae
Bepya	*Cratoxylum neriifolium* Kurz	Hypericaceae
Binga	*Mitragyna rotundifolia* (Roxb.) Kuntze	Rubiaceae
Chinyoke	*Garuga pinnata* Roxb.	Burseraceae
Danyin	*Abarema bigemina* (L.) I.C.Nielsen	Leguminosae
Didu	*Bombax insigne* Wall.	Bombacaceae
Dwabok	*Kydia calycina* Roxb.	Malvaceae
Gwe	*Spondias mangifera* Willd.	Anacardiaceae
Gyo	*Schleichera oleosa* (Lour) Oken.	Sapindaceae
Hman	*Xeromphis spinose* Lamk.	Rubiaceae
Htamachauk	*Gomphostemma lucidum* Wall.ex Benth.	Lamiaceae
Htamasok	*Glochidion glaucifolium* Muell. Arg.	Euphorbiaceae
Htaukshar	*Vitex canescens* Kurz	Lamiaceae
Hteinkala	*Nauclea sessilifolia* Roxb.	Rubiaceae
Kabaung	*Strychnos nux-blanda* A.W.Hill	Loganiaceae
Kalaw	*Gynocardia odorata* R. Br.	Achariaceae
Kanazo	*Heritiera fomes* Wall.	Sterculiaceae

Myanmar Names	Botanical Names	Family Names
Kanyin	*Dipterocarpus alatus* Roxb.	Dipterocarpaceae
Kathit	*Erythrina stricta* Roxb.	Fabaceae
Kaunghmu	*Anisoptera curtisii* Dyer ex King	Dipterocarpaceae
Kokko	*Albizia lebbek* (L.) Benth	Fabaceae
Kuthan	*Hymenodictyon orixense* Mabb.	Rubiaceae
Kyana	*Xylocarpus moluccensis* (Lamk.)M.Roem	Meliaceae
Kyaungsha	*Oroxylum indicum* (L.) Kurz	Bignoniaceae
Kyetmauk	*Litchi chinensis* Sonn.	Sapindaceae
Kyetyo	*Vitex limnifolia* Wall.	Verbenaceae
Kyun	*Tectona grandis* Linn.f.	Verbenaceae
Kyun bo	*Premna pyramidata* Wallich	Verbenaceae
Lein	*Terminalia pyrifolia* Kurz	Combretaceae
Letkok	*Pterygota alata* (Roxb.) R.Br.	Sterculiaceae
Letpan	*Bombax ceiba* L.	Bombacaceae
Leza	*Lagerstroemia tomentosa* Presl.	Lythraceae
Linyaw	*Dillenia parviflora* Griff.	Dilleniaceae
Madama	*Dalbergia ovata* Grah.	Fabaceae
Magyipauk	*Gardenia sessiliflora* Wall.ex C.B.Clarke	Rubiaceae
Mahlwa	*Markhamia stipulate* Seeme.ex K.	Bignoniaceae
Maniauga	*Carallia brachiate* (Lour.) Merr.	Pinaceae
Mau	*Anthocephalus morindifolius* Korth.	Rubiaceae
Mayanin	*Pittosporum napaulensis* Rehder W.	Pittosporaceae
Myaukchaw	*Homolium tomentosum* Benth.	Flacourtiaceae

Myanmar Names	Botanical Names	Family Names
Myaukngo	*Duabanga grandiflora* Walp	Lythraceae
Myaya	*Microcos paniculata* L.	Malvaceae
Nabe	*Lannea coromandelica* (Houtt).Merr.	Anacardiaceae
Nage	*Pterospermum semisagittatum* Buch-Ham.	Sterculiaceae
Ngahlaing bo	*Mallotus repandus*	Euphorbiaceae
Ngu	*Cassia fistula* L.	Fabaceae
Ondon	*Litsea glutinosa* (Lour) C.B.Rob.	Lauraceae
Padauk	*Pterocarpus macrocarpus* Kurz	Leguminosae
Panga	*Terminalia chebula* Retz.	Combretaceae
Pauk	*Butea monosperma* (Lam.) Kuntze	Fabaceae
Phet-kyan	*Quercus lindleyana* Wall.	Fagaceae
Phetthan	*Heterophragma adenophyllum* Wall	Bignoniaceae
Phetwun	*Berrya mollis* Wall.ex Kurz	Tiliaceae
Pokethinma	*Derris robusta* (Roxb. ex DC.) Benth.	Fabaceae
Pyaukseik	*Holoptelea integrifolia* Planch.	Ulmaceae
Pyinkado	*Xylia xylocarpa* (Roxb.) Toub.	Mimosaceae
Pyinma	*Lagerstroemia speciose* (L.) Pers.	Lythraceae
Sawbya	*Sterculia campanulata* Wall.	Sterculiaceae
Seikchi	*Bridelia retusa* (L.) A.Juss.	Euphorbiaceae
Shaw	*Sterculia angustifolia* Jack	Sterculiaceae
Sit	*Albizzia procera* (Roxb.) Benth.	Mimosaceae
Swedaw	*Bauhinia acuminate* L.	Fabaceae
Taukkyant	*Terminalia crenulata* (Heyne) Roth	Combretaceae

Myanmar Names	Botanical Names	Family Names
Taung-gangaw	*Mesua nervosa*	Guttiferae
Taung-gwe	*Spondias pinnata* (L.) Kurz.	Anacardiaceae
Taunggyi	*Barringtonia racemose* (L.) Spreng	Barringtoniaceae
Taung-karamet	*Cordia fragrantissima* Kurz	Boraginaceae
Taung-khaya	*Dialium indum* Noronh.	Leguminosae
Taung-kyetmauk	*Xerospermum noronhianum* Blume	Sapindaceae
Taung-mayo	*Alstonia scholaris* R.Br.	Apocynaceae
Taung-nage	*Pterospermum lanceifolium* Roxb.	Sterculiaceae
Taung-ohnshit	*Arenga saccharifera* Labill.	Arecaceae
Taung-peinne	*Artocarpus chaplasha* Roxb.	Moraceae
Taung-phetwun	*Pterospermum acerifolium* Willd	Sterculiaceae
Taung-thayet	*Mangifera caloneura* Kurz	Anacardiaceae
Taw-shaut	*Citrus medica* L.	Rutaceae
Thabye	*Syzygium tetragonum* (L.) Skeels.	Myrtaceae
Thadi	*Protium serratum* Engl.	Burseraceae
Thakhut	*Dolichandrone serrulata* Seem.	Bignoniaceae
Thakhutpo	*Stereospermum fimbriatum* DC.	Bignoniaceae
Thanakha	*Hesperethusa crenulata* (Roxb.)Roem	Rutaceae
Thande	*Stereospermum colais* Mabb.	Bignoniaceae
Thanzat	*Albizia lucidior* Nielsen	Mimosaceae
Thaputgyi	*Miliusa velutina* Hool.f.&Thomson	Annonaceae
Thayet	*Mangifera indica* L.	Anacardiaceae
Thayingyi	*Croton roxburghianus* N.P.Balakr	Euphorbiaceae

Myanmar Names	Botanical Names	Family Names
Thingadu	*Parashorea stellata* Kurz	Dipterocarpaceae
Thinwin	*Millettia pendula* Benth.	Fabaceae
Thitkala	*Pentace griffithii* King	Tiliaceae
Thitmagyi	*Albizia odoratissima* (L.f.)Benth.	Mimosaceae
Thitnima	*Amoora cucullata* Roxb.	Meliaceae
Thitpagan	*Millettia brandisiana* Kurz	Fabaceae
Thitpayaung	*Lophopetalum wallichii* Kurz	Celastraceae
Thitpok	*Dalbergia kurzii* Prain	Fabaceae
Thitpyu	*Wendlandia glabrata* DC	Rubiaceae
Thitsat	*Beilschmiedia roxburghiana* Wall.	Lauraceae
Thitseint	*Terminalia belerica* Roxb.	Combretaceae
Thitsi	*Melanorrhea usitata* Wall.	Anacardiaceae
Thitwa	*Linociera terniflora* Wall.	Oleaceae
Wunthaechay	*Lithocarpus kingianus* (Gamble)A.Camus	Fagaceae
Yemane	*Gmelina arborea* Roxb.	Verbenaceae
Yindaik	*Dalbergia cultrata* Grah.	Leguminosae
Yinzat	*Dalbergia fusca* Pierre	Fabaceae
Yon	*Anogeissus acuminata* Wall.	Combretaceae
Zaungbale	*Lagerstroemia villosa* Wall.ex.Kurz	Lythraceae
Zepyu	*Emblica officinalis* Gaertn.	Euphorbiaceae
Zinbyun	*Dillenia pentagyna* Roxb.	Dilleniaceae

Appendix 2

List of species found inside 10m x 10m plots of South Zarmani Reserved Forest

Myanmar Names	Botanical Names	Family Names
Aukchinsa	*Amoora wallichii* King	Meliaceae
Bamaw	*Elaeocarpus wallichii* Kurz	Elaeocarpaceae
Bepya	*Cratoxylum neriifolium* Kurz	Hypericaceae
Binga	*Mitragyna rotundifolia* (Roxb.) Kuntze	Rubiaceae
Chinyoke	*Garuga pinnata* Roxb.	Burseraceae
Danyin	*Abarema bigemina* (L.) I.C.Nielsen	Leguminosae
Didu	*Bombax insigne* Wall.	Bombacaceae
Gwe	*Spondias mangifera* Willd.	Anacardiaceae
Gyo	*Schleichera oleosa* (Lour) Oken.	Sapindaceae
Htamachauk	*Gomphostemma lucidum* Wall.ex Benth.	Lamiaceae
Htamasok	*Glochidion glaucifolium* Muell. Arg.	Euphorbiaceae
Htaukshar	*Vitex canescens* Kurz	Lamiaceae
Kabaung	*Strychnos nux-blanda* A.W.Hill	Loganiaceae
Kalaw	*Gynocardia odorata* R. Br.	Achariaceae
Kanazo	*Heritiera fomes* Wall.	Sterculiaceae
Kanyin	*Dipterocarpus alatus* Roxb.	Dipterocarpaceae
Kaunghmu	*Anisoptera curtisii* Dyer ex King	Dipterocarpaceae
Kyetmauk	*Litchi chinensis* Sonn.	Sapindaceae
Kyetyo	*Vitex limnifolia* Wall.	Verbenaceae
Kyun	*Tectona grandis* Linn.f.	Verbenaceae

Myanmar Names	Botanical Names	Family Names
Lein	*Terminalia pyrifolia* Kurz	Combretaceae
Letkok	*Pterygota alata* (Roxb.) R.Br.	Sterculiaceae
Madama	*Dalbergia ovata* Grah.	Fabaceae
Magyipauk	*Gardenia sessiliflora* Wall.ex C.B.Clarke	Rubiaceae
Mahlwa	*Markhamia stipulate* Seeme.ex K.	Bignoniaceae
Mau	*Anthocephalus morindifolius* Korth.	Rubiaceae
Mayanin	*Pittosporum napaulensis* Rehder W.	Pittosporaceae
Myaukchaw	*Homolium tomentosum* Benth.	Flacourtiaceae
Myaukngo	*Duabanga grandiflora* Walp	Lythraceae
Myaya	*Microcos paniculata* L.	Malvaceae
Nabe	*Lannea coromandelica* (Houtt).Merr.	Anacardiaceae
Nage	*Pterospermum semisagittatum* Buch-Ham.	Sterculiaceae
Ngahlaing bo	*Mallotus repandus*	Euphorbiaceae
Ngu	*Cassia fistula* L.	Fabaceae
Panga	*Terminalia chebula* Retz.	Combretaceae
Phet-kyan	*Quercus lindleyana* Wall.	Fagaceae
Phetthan	*Heterophragma adenophyllum* Wall	Bignoniaceae
Phetwun	*Berrya mollis* Wall.ex Kurz	Tiliaceae
Pokethinma	*Derris robusta* (Roxb. ex DC.) Benth.	Fabaceae
Pyinkado	*Xylia xylocarpa* (Roxb.) Toub.	Mimosaceae
Pyinma	*Lagerstroemia speciose* (L.) Pers.	Lythraceae
Sawbya	*Sterculia campanulata* Wall.	Sterculiaceae
Seikchi	*Bridelia retusa* (L.) A.Juss.	Euphorbiaceae

Myanmar Names	Botanical Names	Family Names
Sit	*Albizzia procera* (Roxb.) Benth.	Mimosaceae
Taukkyant	*Terminalia crenulata* (Heyne) Roth	Combretaceae
Taung-gangaw	*Mesua nervosa*	Guttiferae
Taunggyi	*Barringtonia racemose* (L.) Spreng	Barringtoniaceae
Taung-khaya	*Dialium indum* Noronh.	Leguminosae
Taung-mayo	*Alstonia scholaris* R.Br.	Apocynaceae
Taung-nage	*Pterospermum lanceifolium* Roxb.	Sterculiaceae
Taung-ohnshit	*Arenga saccharifera* Labill.	Arecaceae
Taung-phetwun	*Pterospermum acerifolium* Willd	Sterculiaceae
Taung-thayet	*Mangifera caloneura* Kurz	Anacardiaceae
Taw-shaut	*Citrus medica* L.	Rutaceae
Thabye	*Syzygium tetragonum* (L.) Skeels.	Myrtaceae
Thadi	*Protium serratum* Engl.	Burseraceae
Thakhut	*Dolichandrone serrulata* Seem.	Bignoniaceae
Thakhutpo	*Stereospermum fimbriatum* DC.	Bignoniaceae
Thande	*Stereospermum colais* Mabb.	Bignoniaceae
Thanzat	*Albizia lucidior* Nielsen	Mimosaceae
Thaputgyi	*Miliusa velutina* Hool.f.&Thomson	Annonaceae
Thayingyi	*Croton roxburghianus* N.P.Balakr	Euphorbiaceae
Thinwin	*Millettia pendula* Benth.	Fabaceae
Thitkala	*Pentace griffithii* King	Tiliaceae
Thitpagan	*Millettia brandisiana* Kurz	Fabaceae
Thitpyu	*Wendlandia glabrata* DC	Rubiaceae

Myanmar Names	Botanical Names	Family Names
Thitsat	*Beilschmiedia roxburghiana* Wall.	Lauraceae
Thitseint	*Terminalia belerica* Roxb.	Combretaceae
Yindaik	*Dalbergia cultrata* Grah.	Leguminosae
Yinzat	*Dalbergia fusca* Pierre	Fabaceae
Yon	*Anogeissus acuminata* Wall.	Combretaceae
Zepyu	*Emblica officinalis* Gaertn.	Euphorbiaceae
Zinbyun	*Dillenia pentagyna* Roxb.	Dilleniaceae

위성영상과 지상부 바이오매스 자료를 이용한 미안마 방고 요마 지역의 열대림 지상부 바이오매스 추정

최근 환경보존의 중요성에 대한 인식 증가에도 불구하열대우림의 파괴로 인한 대기 중 이산화탄소배출은 중요한 문제이다. 특히, 열대림의 지상부바이오매스(Above Ground Biomass, AGB)는 전지구적 탄소저감의 중요한 역할을 한다. 따라서 변화하고 있는 열대림 AGB의 정확한 측정이 중요하다. 미얀마의 산림보전의 일환으로 Bago Yoma 지역 Zarmani 보존림 남쪽에 100개의 실험구를 설치하여 AGB를 측정 후, Landsat 8 Operational Land Imager (OLI)와 측정값을 이용 하여 추정한 값과 비교였다. 다중선형회귀분석(Multi Linear Regression, MLR)값과 주성분분석(Principal Component Analysis, PCA)은 Landsat 위성 이미지와 분광 반사율(spectral reflectance), 고도를 입력 변수로 이용하여 AGB 추정을 위하여 개발하였다. MLR은 r^2 = 0.43, RMSE (Root Mean Square Error) = 60.2 tons ha^{-1} 로 RMSE = 70.1%, Bias = -9.1 tons ha^{-1}, Bias (%) = -10.6%를 나타냈고, 반면 PCA는 r^2 = 0.45, RMSE

= 55.1 tons ha^{-1}, RMSE = 64.1%, Bias = -8.3 tons ha^{-1}, Bias (%) = -9.7%, p < 0.0001 을 나타내었다. 실험대상지의 AGB 지도는 MLR과 PCA를 이용하여 생성하였다. AGB의 예상 추정값은 74.74 ± 22.3 tons ha^{-1}, 73.04 ± 17.6 tons ha^{-1} 으로 실험지의 총 AGB는 MLR과 PCA에서 각각 약 5.7만 톤, 5.6만 톤 으로 각각 나타났다. 본 연구는 미얀마의 Bago Yoma 지역 Zarmani 보존림 남쪽 지역을 대상으로 Landsat 8 OLI 이미지와 실측자료를 이용하여 AGB 추정 회귀모델을 생성하였고, 이 모델을 이용한 AGB 추정은 2%이내로 가능하다.

주요어: 지상부 바이오매스, Landsat 8 OLI, 다중선형회귀분석(MLR), 주성분분석(PCA), 열대 활엽수림

학 번: 2013-23876